Solar Energy Materials and Solar Cells 170 (2017) 8–12

Contents lists available at ScienceDirect

Solar Energy Materials and Solar Cells

journal homepage: www.elsevier.com/locate/solmat

Improved electronic transport properties of tin-halide perovskites

G.R. Berdiyorov*, M.E. Madjet, F. El-Mellouhi

Qatar Environment and Energy Research Institute, Hamad bin Khalifa University, Qatar Foundation, Doha, Qatar

ARTICLE INFO

Keywords:
Hybrid perovskite
Electronic transport
Green's functions
Density functional theory

ABSTRACT

Density functional theory in combination with the nonequilibrium Green's function formalism is used to study the electronic transport properties of $MAPbI_3$, $MASnI_3$ and mixed-$MAPb_{0.5}Sn_{0.5}I_3$ perovskites (MA–methylammonium). The largest electronic transport is obtained for tin-halide sample due to the delocalization of electronic states in the system. The mixed sample also shows improved transport properties as compared to the lead-halide system. In addition, tin-based perovskites are less sensitive to the spin-orbit interactions, whereas the electronic transport properties of $MAPbI_3$ are strongly affected by the relativistic effects. These findings indicate the possibility of enhancing charge carrier transport in organometallic perovskites by metal atom mixing.

1. Introduction

Organometallic halide perovskites, such as methylammonium (MA) lead iodide ($MAPbI_3$), emerged as a potential light harvesting materials with the solar conversion efficiency already exceeding 20% (see Refs. [1–6] for reviews). An excellent performance of perovskite-based solar cells is related to relatively long carrier diffusion length, relatively high mobility of charge carriers, low exciton binding energy, and optimum band gap and band alignment enabling strong photon absorption across most of the solar spectrum [7–9]. Moreover, photoconversion efficiency of the hybrid halide perovskites can be further improved by modifying the composition of different components (organic compounds, halogens and metal atoms) [10–22]. Besides the long term operational stability issues [23–25] related to, e.g., the negative influence of humidity and ultraviolet radiation, the development of efficient lead-free hybrid perovskite materials with reduced toxicity has become one of the main objectives in the research community.

Replacement of lead with different homovalent metal ions is considered to be an effective tool of reducing the potential environmental impact of lead-based perovskites [26,27]. Fundamental understanding of the role of lead-replacing metal atoms in the archetypical material is of great importance in developing low-toxicity lead-free perovskite solar cell [28]. Among the other transition metals, tin (Sn) is considered to be one of possible candidates as a replacement for lead [29–36]. Partial replacement of Pb^{2+} with Sn^{2+} lowers the band gap thus extending the absorption spectra towards the mid-infrared region of the solar spectrum [31,37–42]. The structural properties of the material are also affected by partial Pb-Sn substitutions [34], which in turn influences the optoelectronic and transport properties of the mixed material [43,44]. Despite such a tunability of the bandgaps, the solar-conversion efficiency tin-based perovskites is much lower as compared the one of lead-based perovskites, which is related to several factors such as poor semiconductor quality, low surface coverage [39,45,46] and the instability due to the oxidation of Sn^{2+} to Sn^{4+}. The latter represents one of the main mechanism for the decomposition of tin-based perovskites [31]. The relatively high background dark carrier density was also shown to be responsible for the lower photovoltaic power conversion efficiency of the Sn-based perovskite as compared to its Pb-based analogues [47]. Defect tolerance of these hybrid materials is also one of the important factors affecting the performance of perovskite based solar cells. However, higher efficiency of the mixed Sn-Pb halide perovskite solar cells can be achieved by carefully designing the crystal structure of the material [48–51]. The highest efficiency was reported for $MAPb_{0.75}Sn_{0.25}I_3$ perovskite (14.12%), which is the most efficient solar cell based on Sn-based perovskite material [50]. Small improvement in the photoconversion efficiency (14.19%) was obtained for mixed-cation Sn-based perovskite, $MA_{0.5}FA_{0.5}Pb_{0.75}Sn_{0.25}I_3$ [51]. Eperon et al., reported the efficiency of 14.8% for another mixed-cation material $FA_{0.75}Cs_{0.25}Pb_{0.5}Sn_{0.5}I_3$ [52]. The efficiency can be increased further by creating lead- and tin-based perovskite heterostructures with graded bandgap [51–53].

Despite such extensive research, electronic transport properties of mixed-Pb-Sn halide perovskites are relatively little understood [9]. From the other hand, high charge carrier mobilities are key to the photovoltaic performance of solar cell devices. Therefore, in this work we employ density-functional theory (DFT) in combination with the

* Corresponding author.
E-mail address: gberdiyorov@hbku.edu.qa (G.R. Berdiyorov).

http://dx.doi.org/10.1016/j.solmat.2017.05.045
Received 29 December 2016; Received in revised form 16 May 2017; Accepted 17 May 2017
Available online 25 May 2017

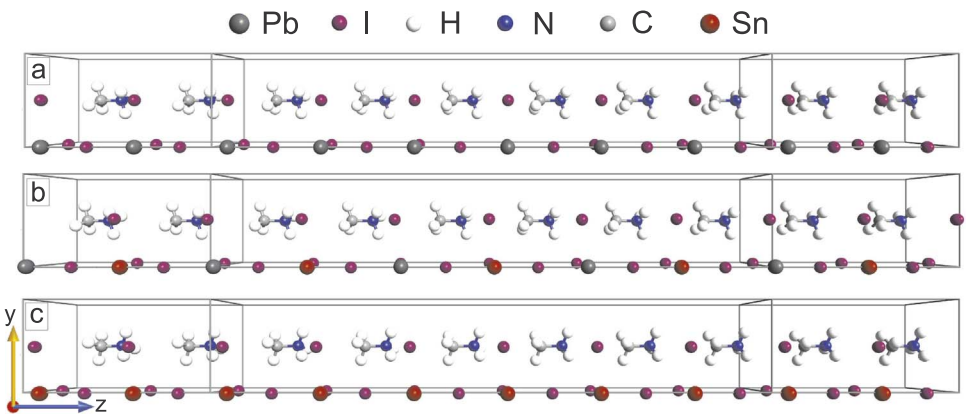

Fig. 1. Device geometries: cubic lattice structure of $CH_3NH_3PbI_3$ (a), $CH_3NH_3Pb_{0.5}Sn_{0.5}I_3$ (b) and $CH_3NH_3SnI_3$ (c). Periodic boundary conditions are applied along the *x*- and *y*-directions and electronic transport is calculated along the *z*-direction through the metallic electrodes.

nonequilibrium Green's function formalism to study the electronic transport properties of mixed-$MAPb_{0.5}Sn_{0.5}I_3$ perovskite (see Fig. 1(b)). The choice of this Sn-concentration is motivated by the fact that this material has the broadest light absorption and highest short-circuit photocurrent density among the other lead and tin mixed halides [38]. As a reference, we also study the electronic transport in $MAPbI_3$ (Fig. 1(a)) and $MASnI_3$ (Fig. 1(c)) samples. We consider the cubic crystalline phases of all three systems [43,54] in order to reduce the geometric changes induced by the organic cation. In addition, the Pb and Sn mixture can be obtained in such high-temperature cubic phase for all halide compounds [55]. We found that the mixed sample also shows enhanced electronic transport as compared to $MAPbI_3$. However, the largest electronic transmission is obtained for $MASnI_3$ sample: the ballistic current obtained from quantum transmission calculations can be an order of magnitude higher as compared to the other systems. The obtained results can be explained in terms of electronic states localization and variations of the electrostatic potential.

2. Computational details

Geometry optimizations were performed using DFT within the generalized gradient approximation of Perdew-Burke-Ernzerhof (PBE) to represent the exchange-correlation energy [56]. The Brillouin zone sampling was performed using $6\times6\times6$ *k*-points [57]. van der Waals interactions, which are known to be important for the structural properties of organo-metallic perovskites [10], were taken into account using Grimme's DFT-D3 empirical dispersion correction to the PBE [58]. Both atomic coordinates and lattice parameters are fully relaxed during the simulations. Calculations are performed using the Vienna ab initio simulation package (VASP) [59,60]. Lattice parameters and atomic positions from the VASP calculations were used to calculate the electronic transport using the computational package Atomistix toolkit [61]. The electronic structure was obtained self-consistently within the DFT/PBE and the electrostatic potentials were defined on a real-space grid with a mesh cutoff energy of 150 Ry. Norm conserving OpenMX pseudopotential with high basis sets were employed for all atoms (Pb: s2p2d2f1, Sn: s2p2d2f1, I: s2p2d1, N: s2p2d1, C: s2p2d1, and H: s2p1). The spin-orbit coupling effects were taken into account within the noncollinear magnetism framework. Note that the present method does not account for electron-phonon interactions. Note also that in order to have the band alignment of the electrodes, the energy is measured relative to the average Fermi level of the two electrodes. These Fermi levels are, in turn, aligned with the applied bias on each electrode. We have monitored the energy resolved spectral current in order to have enough energy range for the evaluation of the transmission spectra.

3. Results and discussions

Our starting geometry was the cubic structure of $MAPbI_3$ with MA molecules oriented along the 100 direction relative to the origin of the lattice. The geometry optimization gives a pseudocubic lattice with parameters 6.313 Å × 6.313 Å × 6.317 Å, which is close to the experimental value of 6.33 Å [62]. Full replacement of Pb with Sn also gives us a pseudocubic unit cell with smaller lattice parameters 6.226 Å × 6.226 Å × 6.227 Å. Finally, the mixed-$MAPb_{0.5}Sn_{0.5}I_3$ sample has a unit cell with lattice parameters 6.309 Å × 6.309 Å × 12.627 Å. On the base of the obtained lattice structures, we have constructed devise geometries (see Fig. 1), each of which consists of left and right regions (i.e., electrodes), which are connected to a central region (i.e. two-probe configuration). The thickness of the electrodes are 12.634 Å, 12.627 Å, and 12.454 Å, respectively for $MAPbI_3$, $MAPb_{0.5}Sn_{0.5}I_3$ and $MASnI_3$ samples. The length of the scattering region is three times longer than the length of the electrodes. The electronic transport through the system is calculated using the nonequilibrium Green's function formalism with the $6\times6\times100$ *k*-point sampling.

Fig. 2(a) shows the zero bias transmission spectra, $T(E)$, as a function of the electron energy for all three considered samples. These

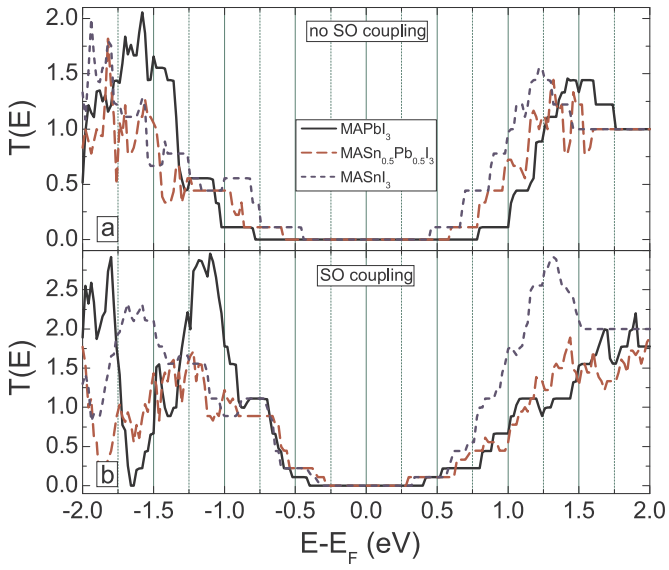

Fig. 2. Zero bias transmission spectra as a function of electron energy (the Fermi energy is taken at $E=0$) for $CH_3NH_3PbI_3$ (solid-black curves), $CH_3NH_3Pb_{0.5}Sn_{0.5}I_3$ (dashed-red curves) and $CH_3NH_3SnI_3$ (dotted-blue curves). The results are obtained without (a) and with (b) the spin-orbit coupling. In (b) the results are the sum for spin up and spin down electrons. (For interpretation of the references to color in this figure legend, the reader is referred to the web version of this article.)